Site-bond percolation in two-dimensional kagome lattices: Analytical approach and numerical simulations

M. I. González-Flores [2], A. A. Torres [1], W. Lebrecht [2], and A. J. Ramirez-Pastor [1,*]

[1]*Departamento de Física, Instituto de Física Aplicada (INFAP), Universidad Nacional de San Luis–CONICET, Ejército de Los Andes 950, D5700HHW San Luis, Argentina*

[2]*Departamento de Física, Universidad de La Frontera, Casilla 54-D, Temuco, Chile*

(Received 8 May 2021; accepted 21 June 2021; published 23 July 2021)

The site-bond percolation problem in two-dimensional kagome lattices has been studied by means of theoretical modeling and numerical simulations. Motivated by considerations of cluster connectivity, two distinct schemes (denoted as $S \cap B$ and $S \cup B$) have been considered. In $S \cap B$ ($S \cup B$), two points are connected if a sequence of occupied sites *and* (*or*) bonds joins them. Analytical and simulation approaches, supplemented by analysis using finite-size scaling theory, were used to calculate the phase boundaries between the percolating and nonpercolating regions, thus determining the complete phase diagram of the system in the (p_s, p_b) space. In the case of the $S \cap B$ model, the obtained results are in excellent agreement with previous theoretical and numerical predictions. In the case of the $S \cup B$ model, the limiting curve separating percolating and nonpercolating regions is reported here.

DOI: 10.1103/PhysRevE.104.014130

I. INTRODUCTION

Since its introduction in the 1950's [1,2], the percolation theory has been a focal point of statistical mechanics and it has been applied to a wide range of phenomena, such as flow in porous materials [3–5], conductive materials [6,7], networks [8–11], colloids [12], the spin quantum Hall transition [13], and the spread of epidemics [14]. Percolation is also a fundamental model in the statistical mechanics of phase transitions and critical phenomena [3,4,15–17].

Usually, the percolation model in a lattice is classified into two categories, namely, the site model and the bond model [3]. In the site [bond] model, vertices [edges] of a lattice in dimension d are independently occupied with probability p_s [p_b] or empty (nonoccupied) with probability $1 - p_s$ [$1 - p_b$]. Nearest-neighboring occupied sites (bonds) form structures called clusters. For an infinite lattice, there is a critical probability p_{sc} [p_{bc}], above which a cluster extends from one side of the system to the other. This cluster is called the infinite cluster, and its presence determines a geometrical phase transition in the system. Finding the critical point p_{sc} [p_{bc}] is central to many theoretical and computational studies of percolation.

The original site (bond) percolation model has spawned many generalizations. Among them, the site-bond percolation problem has received considerable attention in various areas [3,4,15,18–24]. In this framework, sites and bonds are randomly and independently occupied with occupancy fractions p_s and p_b, respectively. It is possible then to define *site-and-bond* ($S \cap B$) and *site-or-bond* ($S \cup B$) percolation: in $S \cap B$ ($S \cup B$), two points are said to be connected if a sequence of occupied sites *and* (*or*) bonds joins them. Thus, in $S \cap B$, a cluster is considered to be a set of occupied bonds and sites in which the bonds are joined by occupied sites, and the sites are joined by occupied bonds. In $S \cup B$, a bond or site contributes to cluster connectivity independently of the occupation of its end points.

The site-bond percolation problem has many applications in different fields. For instance, it has been used as a prototype model to study the sol-to-gel transition (gelation) of polymers [25]. In this model, bonds represent chemical bonds, occupied sites represent monomers, and empty sites represent solvent molecules. The site-bond percolation has also been applied to study dissociative adsorption on metal surfaces [26,27]. In this sense, Gao and Yang [28] investigated the process of dissociative adsorption of dimers and studied the percolating properties of the dissociated monomers as a function of both the concentration of dimers (sites) and the dissociation probability (bonds). A phase diagram separating a percolating from a nonpercolating region was obtained. Biological and medical applications have invoked the mixed percolation case. A typical example arises when some pathological condition spreads by contagious infection through a large static colony of biological cells (or individuals), of which a proportion p is susceptible and a proportion $1 - p$ is immune to the infection. The cells are the vertices of a lattice (sites), and the edges of the lattice (bonds) connect pairs of neighboring cells, between which infection may spread [29]. The traditional approach of site-bond percolation has been used to model pore network structure and capillary phenomena. In this framework, sites represent pore bodies (cavities) and bonds correspond to pore necks (windows) [30–32].

Here, we discuss a version of two-dimensional (2D) percolation on the kagome lattice. The kagome lattice is of great interest to the physics community because it manifests geometric frustration (the phenomenon of having a large

*antorami@unsl.edu.ar

number of degenerate ground states for geometric reasons). In the field of magnetism, the antiferromagnetic kagome lattice may be the most frustrated 2D magnetic system that one can construct [33]. Kagome antiferromagnets are central in the search for exotic quantum states because both the spin and the charge are frustrated geometrically, enabling the formation of spin-liquid phases and topological electronic structures [34–36]. Kagome ferromagnets also provide unusual physics, showing large anomalous Hall effects that can arise from nontrivial electronic topology with nonvanishing Berry curvatures [37–39].

From the perspective of percolation theory, the problems of pure site percolation, pure bond percolation, and $S \cap B$ mixed percolation on kagome lattices have been studied by means of numerical simulations and analytical approaches [21–23,40–46]. Relevant details of these papers will be reviewed in Secs. II and IV. The $S \cup B$ model has received considerably less attention in the literature [47–51]. In particular, the critical curve corresponding to the $S \cup B$ problem on kagome lattices has not yet been reported.

Despite previous work, site-bond percolation in kagome lattices has resisted exact calculations and, accordingly, there are no known exact results for the critical lines separating the percolating and nonpercolating regions in the $S \cap B$ and $S \cup B$ models. In this context, the development of numerical simulations and analytically solvable models might be a help and a guide to identify and characterize the most prominent features of this kind of systems. The main objective of this paper is to provide a thorough study in this direction. For this purpose, a theoretical framework is presented based upon (i) the classical Tsallis approximation [52], which allows us to calculate the $S \cap B$ and $S \cup B$ percolation functions from the percolation functions corresponding to pure site and pure bond percolation problems; and (ii) the analytical percolation functions obtained by Scullard and Ziff (pure bond percolation model) [42], Sykes and Essam (pure site percolation model) [45], and Rosowsky (pure site percolation model) [46]. In addition, extensive computer simulations are performed in order to test the validity of the theoretical model. In the case of the $S \cap B$ model, the results obtained here are compared with previous theoretical and numerical predictions [21–23]. In the case of the $S \cup B$ model, the complete percolation phase diagram is reported here.

The paper is organized as follows. The theoretical approach is introduced in Sec. II, which includes the main results concerning the phase diagrams obtained from the analytical calculations. Details of the calculations are given in the Appendix. Simulation calculations are described in Sec. III. In Sec. IV, the analytical predictions are compared with simulation data and previous results in the literature [21–23]. Finally, the conclusions are drawn in Sec. V.

II. ANALYTICAL APPROACH

The kagome lattice is one of the fundamental lattices of 2D percolation, as well as many other 2D lattice problems. It is one of the 11 Archimedean tiling lattices, which are vertex-transitive graphs made in two dimensions by edge-to-edge tiling of regular polygons, the vertices of which are surrounded by the same sequence of polygons [53].

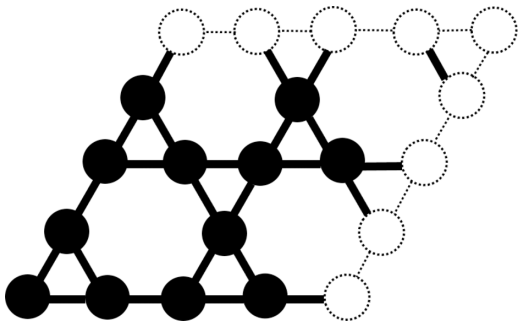

FIG. 1. Schematic diagram of a kagome lattice composed of four unit cells. Solid circles and thick segments represent sites and bonds in the lattice, respectively. Dashed open circles and dashed segments denote boundary sites and bonds, respectively.

The Archimedean lattices are categorized in terms of the set of polygons which surround each vertex, $({n_1}^{a_1}, {n_2}^{a_2}, \dots)$ [53]. Going clockwise around a vertex, the numbers n_i denote the number of sides of each polygon, and the superscript a_i refers to the number of these polygons adjacent to each other. In the case of the kagome lattice, each vertex touches a triangle, a hexagon, a triangle, and a hexagon. Accordingly, the corresponding notation is (3,6,3,6).

A schematic diagram of a kagome lattice is shown in Fig. 1, where each site (solid circle) corresponds to a vertex of the lattice and each bond (thick segment) corresponds to a polygon side. Four unit cells are represented in Fig. 1. Each unit cell contains three sites and six bonds. Dashed open circles and dashed segments represent boundary sites and bonds, respectively. The concept of a unit cell has been previously used to calculate bond percolation thresholds in Archimedean lattices [41–44].

As mentioned in Sec. I, our idea is to address the site-bond percolation problem on the kagome lattice. In this scheme, sites and bonds are randomly and independently occupied with occupancy fractions p_s and p_b, respectively. It is possible then to define *site-and-bond* ($S \cap B$) and *site-or-bond* ($S \cup B$) percolation: in $S \cap B$ ($S \cup B$), two points are connected if a sequence of occupied sites *and* (*or*) bonds joins them. Then, in $S \cap B$, a cluster is a set of occupied bonds and sites in which the bonds are joined by occupied sites, and the sites are joined by occupied bonds. In $S \cup B$, a bond or site contributes to cluster connectivity independently of the occupation of its end points. The central idea of the site-bond percolation theory is based on finding the minimum concentration of elements (sites and bonds) for which a cluster extends from one side to the opposite one of the lattice, and a second order phase transition occurs in the system.

It is well known that it is quite a difficult matter to analytically determine the value of the $S \cap B$ and $S \cup B$ percolation thresholds for a given lattice [3]. However, several attempts were made to solve the site-bond percolation problem. Among them, an important contribution to the understanding of the site-bond statistics was made by Tsallis [52], who proposed to calculate the $S \cap B$ and $S \cup B$ percolation functions from the corresponding pure site and pure bond percolation functions.

In the Tsallis scheme [52],

$$h^{S\cap B}(p_s, p_b) = f(p_s)g(p_b) \tag{1}$$

and

$$h^{S\cup B}(p_s, p_b) = f(p_s) + g(p_b) - f(p_s)g(p_b), \tag{2}$$

where $f(p_s)$ [$g(p_b)$] represents the percolation function corresponding to the pure site [bond] percolation problem, and $h^{S\cap B}(p_s, p_b)$ [$h^{S\cup B}(p_s, p_b)$] indicates the percolation function corresponding to the $S \cap B$ [$S \cup B$] percolation problem. Interested readers are referred to Ref. [52] (p. 720) for a more complete description of the Tsallis scheme.

In the case of the kagome lattice, different approximations have been developed to determine the functions $f(p_s)$ and $g(p_b)$. From the analysis of the unit cell and symmetry considerations, Scullard and Ziff [42] derived the critical condition for the bond percolation problem in the kagome lattice,

$$1 - 3p_b^2 - 6p_b^3 + 12p_b^4 - 6p_b^5 + p_b^6 = 0, \tag{3}$$

where the solution $p_{bc} = 0.524\,429\,717\,5\ldots$ in [0,1] is the percolation threshold of the pure bond percolation problem in the kagome lattice. By integrating two times the function in Eq. (3) and applying normalization conditions, we get the corresponding percolation function:

$$g_{\mathrm{SZ}}(p_b) = \tfrac{40}{9}\left(\tfrac{1}{56}p_b^8 - \tfrac{1}{7}p_b^7 + \tfrac{2}{5}p_b^6 - \tfrac{3}{10}p_b^5 - \tfrac{1}{4}p_b^4 + \tfrac{1}{2}p_b^2\right). \tag{4}$$

The subscript SZ in Eq. (4) refers to calculations by Scullard and Ziff [42]. Note that the percolation function $g_{\mathrm{SZ}}(p_b)$ is a positive, increasing, and continuous function on $0 \leqslant p_b \leqslant 1$ with $g_{\mathrm{SZ}}(0) = 0$ and $g_{\mathrm{SZ}}(1) = 1$. The critical threshold $p_{bc} = 0.524\,429\,717\,5\ldots$ can now be determined from the position of the inflection point of $g_{\mathrm{SZ}}(p_b)$.

By using a similar procedure as described for Scullard and Ziff's calculations, $f(p_s)$ can be obtained from the critical conditions derived by Sykes and Essam [45] for the pure bond percolation problem in triangular and honeycomb lattices [54]:

$$1 - 3p_b + p_b^3 = 0 \quad \text{(triangular lattice)} \tag{5}$$

and

$$1 - 3p_b^2 + p_b^3 = 0 \quad \text{(honeycomb lattice)}. \tag{6}$$

The results in the honeycomb lattice also apply to the isomorphic site problem on the kagome lattice. Then, by integrating two times the function in Eq. (6) and normalizing, the percolation function for the site problem on the kagome lattice can be obtained:

$$f_{\mathrm{SE}}(p_s) = \tfrac{1}{6}\left({p_s}^5 - 5{p_s}^4 + 10{p_s}^2\right). \tag{7}$$

In this case, the subscript SE in Eq. (7) refers to calculations by Sykes and Essam [45]. The inflection point of the function $f_{\mathrm{SE}}(p_s)$ denotes the critical threshold for the pure site percolation problem on the kagome lattice $p_{sc} = 0.652\,703\,644\,6\ldots$.

Based on exact counting of configurations on finite cells, an alternative method to calculate $f(p_s)$ was proposed by Rosowsky [46]. The resulting site percolation function, denoted as $f_R(p_s)$, can be written as

$$f_R(p_s) = 3p_s^8 - 8p_s^6 + 6p_s^4. \tag{8}$$

The value of the percolation threshold derived from Eq. (8) is $p_{sc} = 0.654\,653\,6\ldots$.

By following the Tsallis strategy [52] and using the expressions of $g(p_b)$ and $f(p_s)$ in Eqs. (4), (7), and (8), two schemes were used to obtain the site-bond percolation functions.

Scheme 1. $S \cap B$ and $S \cup B$ percolation functions are calculated using $g_{\mathrm{SZ}}(p_b)$ and $f_{\mathrm{SE}}(p_s)$. Thus,

$$h_1^{S\cap B}(p_s, p_b) = f_{\mathrm{SE}}(p_s)g_{\mathrm{SZ}}(p_b). \tag{9}$$

Introducing Eqs. (4) and (7) in Eq. (9), the percolation function is

$$h_1^{S\cap B}(p_s, p_b) = \tfrac{40}{54}\left({p_s}^5 - 5{p_s}^4 + 10{p_s}^2\right)\left(\tfrac{1}{56}p_b^8 - \tfrac{1}{7}p_b^7 + \tfrac{2}{5}p_b^6 - \tfrac{3}{10}p_b^5 - \tfrac{1}{4}p_b^4 + \tfrac{1}{2}p_b^2\right). \tag{10}$$

On the other hand, in the case of $S \cup B$ percolation,

$$h_1^{S\cup B}(p_s, p_b) = f_{\mathrm{SE}}(p_s) + g_{\mathrm{SZ}}(p_b) - f_{\mathrm{SE}}(p_s)g_{\mathrm{SZ}}(p_b), \tag{11}$$

and using Eqs. (4) and (7),

$$\begin{aligned} h_1^{S\cup B}(p_s, p_b) = {} & \tfrac{1}{6}\left({p_s}^5 - 5{p_s}^4 + 10{p_s}^2\right) + \tfrac{40}{9}\left(\tfrac{1}{56}p_b^8 - \tfrac{1}{7}p_b^7 + \tfrac{2}{5}p_b^6 - \tfrac{3}{10}p_b^5 - \tfrac{1}{4}p_b^4 + \tfrac{1}{2}p_b^2\right) \\ & - \tfrac{40}{54}\left({p_s}^5 - 5{p_s}^4 + 10{p_s}^2\right)\left(\tfrac{1}{56}p_b^8 - \tfrac{1}{7}p_b^7 + \tfrac{2}{5}p_b^6 - \tfrac{3}{10}p_b^5 - \tfrac{1}{4}p_b^4 + \tfrac{1}{2}p_b^2\right). \end{aligned} \tag{12}$$

Scheme 2. Site-bond percolation functions are calculated using $g_{\mathrm{SZ}}(p_b)$ and $f_R(p_s)$. Thus,

$$h_2^{S\cap B}(p_s, p_b) = f_R(p_s)g_{\mathrm{SZ}}(p_b). \tag{13}$$

Then,

$$h_2^{S\cap B}(p_s, p_b) = \tfrac{40}{9}\left(3p_s^8 - 8p_s^6 + 6p_s^4\right)\left(\tfrac{1}{56}p_b^8 - \tfrac{1}{7}p_b^7 + \tfrac{2}{5}p_b^6 - \tfrac{3}{10}p_b^5 - \tfrac{1}{4}p_b^4 + \tfrac{1}{2}p_b^2\right). \tag{14}$$

In addition,

$$h_2^{S\cup B}(p_s, p_b) = f_R(p_s) + g_{\mathrm{SZ}}(p_b) - f_R(p_s)g_{\mathrm{SZ}}(p_b), \tag{15}$$

and

$$\begin{aligned} h_2^{S\cup B}(p_s, p_b) = {} & \left(3p_s^8 - 8p_s^6 + 6p_s^4\right) + \tfrac{40}{9}\left(\tfrac{1}{56}p_b^8 - \tfrac{1}{7}p_b^7 + \tfrac{2}{5}p_b^6 - \tfrac{3}{10}p_b^5 - \tfrac{1}{4}p_b^4 + \tfrac{1}{2}p_b^2\right) \\ & - \tfrac{40}{9}\left(3p_s^8 - 8p_s^6 + 6p_s^4\right)\left(\tfrac{1}{56}p_b^8 - \tfrac{1}{7}p_b^7 + \tfrac{2}{5}p_b^6 - \tfrac{3}{10}p_b^5 - \tfrac{1}{4}p_b^4 + \tfrac{1}{2}p_b^2\right). \end{aligned} \tag{16}$$

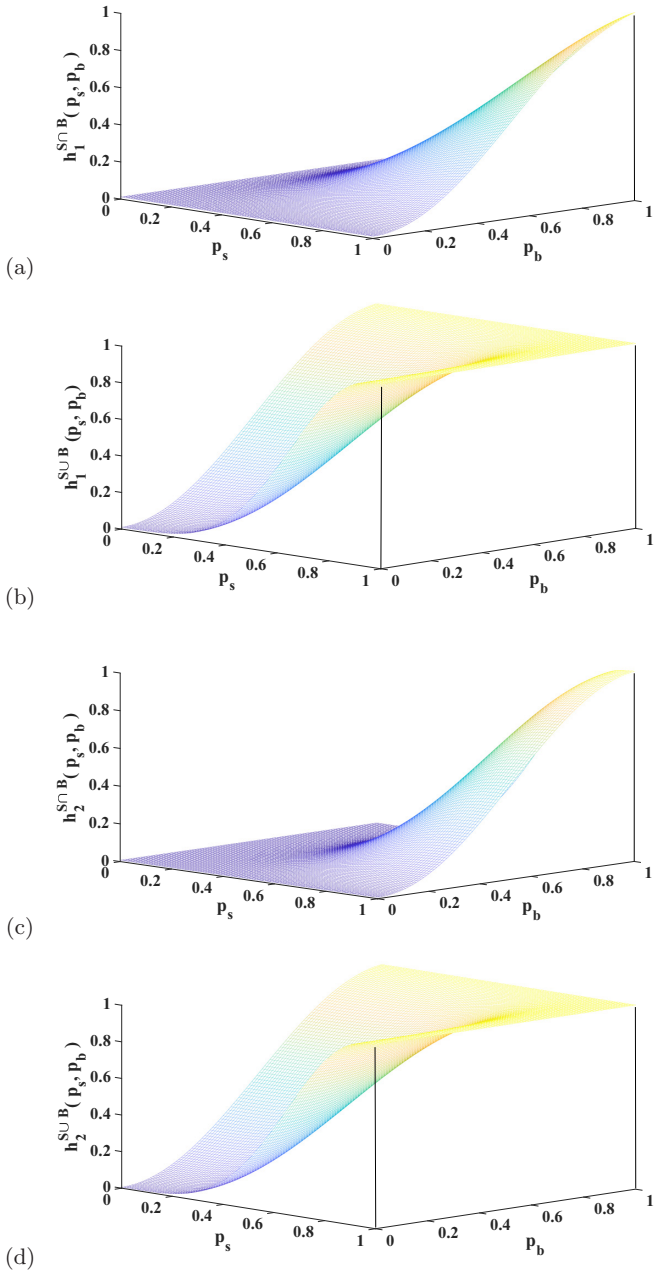

FIG. 2. Percolation functions in the (p_s, p_b) plane: (a) $h_1^{S\cap B}(p_s, p_b)$ [Eq. (10)], (b) $h_1^{S\cup B}(p_s, p_b)$ [Eq. (12)], (c) $h_2^{S\cap B}(p_s, p_b)$ [Eq. (14)], and (d) $h_2^{S\cup B}(p_s, p_b)$ [Eq. (16)].

$h_1^{S\cap B}(p_s, p_b)$ [Eq. (10)], $h_1^{S\cup B}(p_s, p_b)$ [Eq. (12)], $h_2^{S\cap B}(p_s, p_b)$ [Eq. (14)], and $h_2^{S\cup B}(p_s, p_b)$ [Eq. (16)] are plotted in Figs. 2(a)–2(d), respectively. These functions are necessary in order to obtain the critical curves separating the percolating and nonpercolating regions ($p_s - p_b$ phase diagram). For this purpose, the string method [55,56] was used. The procedure is described in the Appendix, and the results are compiled in Table I.

In Sec. IV, the analytical results obtained in the present section will be discussed in comparison with simulation data and previous studies in the literature [21–23].

TABLE I. Values of (p_s, p_b) for the critical line corresponding to the $S \cap B$ and $S \cup B$ percolation models. The data have been obtained by following scheme 1 and scheme 2.

Scheme 1				Scheme 2			
$S \cap B$		$S \cup B$		$S \cap B$		$S \cup B$	
p_b	p_s	p_b	p_s	p_b	p_s	p_b	p_s
0.52443	1.00	0	0.65270	0.52443	1.00	0	0.65465
0.53	0.99434	0.02	0.64782	0.53	0.96140	0.02	0.65445
0.55	0.96447	0.05	0.63875	0.55	0.90150	0.05	0.65348
0.60	0.90235	0.10	0.61124	0.60	0.82434	0.10	0.64971
0.65	0.85974	0.15	0.57810	0.65	0.77486	0.15	0.64213
0.70	0.81457	0.20	0.54264	0.70	0.74045	0.20	0.62848
0.75	0.78013	0.25	0.49566	0.75	0.71139	0.25	0.60589
0.80	0.74703	0.30	0.44694	0.80	0.69103	0.30	0.57201
0.85	0.71467	0.35	0.39231	0.85	0.67618	0.35	0.52550
0.90	0,68823	0.40	0.32956	0.90	0.66585	0.40	0.47431
0.95	0,66845	0.45	0.25289	0.95	0.65917	0.45	0.40150
1.00	0.65270	0.465	0.23052	1.00	0.65465	0.465	0.37549
		0.485	0.18728			0.485	0.33449
		0.50	0.14687			0.50	0.29356
		0.52443	0			0.52443	0

III. SIMULATION METHOD AND RESULTS

Let us consider an initially empty kagome lattice of $L_c \times L_c$ cells, where L_c is the number of unit cells per lattice side ($L_c = 2$ in Fig. 1). Sites and bonds are independently and randomly occupied with concentrations p_s and p_b, respectively. The filling process is as follows: (1) a given site (bond), belonging to the set of empty sites (bonds), is randomly selected and occupied; and (2) the set of empty sites (bonds) is updated. The procedure is repeated until N_s sites and N_b bonds are occupied, and the desired concentrations ($p_s = N_s/M_s$, $p_b = N_b/M_b$) are reached. M_s [M_b] represents the total number of lattice sites [bonds], being $M_s = 3L_c^2$ [$M_b = 6L_c^2$].

Under these considerations, our simulations consist of the following two elementary steps: (a) the construction of the $L_c \times L_c$ kagome lattice for the desired fractions p_s and p_b of occupied sites and bonds, respectively; and (b) the cluster analysis by using the Hoshen and Kopelman algorithm [57] on the occupied elements (sites and bonds) in the lattice [58]. In the last step, the existence of a percolating island is verified.

For each model ($S \cap B$ or $S \cup B$), and for a given size L_c, a value of p_b is chosen. With fixed p_b, steps (a) and (b) are performed for increasing values of p_s until a percolating cluster is formed. By repeating this process n times, the corresponding percolation threshold $p_{s,c}(L_c)$ is obtained. The number n is chosen in order to determine $p_{s,c}(L_c)$ with an uncertainty range between 10^{-4} and 10^{-5}. In the present paper, four lattice sizes were considered: $L_c = 32$, 64, 128, and 256.

With previous results for $p_{s,c}(L_c)$, the infinite percolation threshold $p_{s,c}(\infty) = p_{s,c}$ [for simplicity we will drop the (∞)] can be obtained from scaling analysis [3]. Thus, for each percolation model ($S \cup B$ and $S \cap B$) and for each value of p_b, one expects that

$$p_{s,c}(L_c) = p_{s,c} + A^X L_c^{-1/\nu}, \tag{17}$$

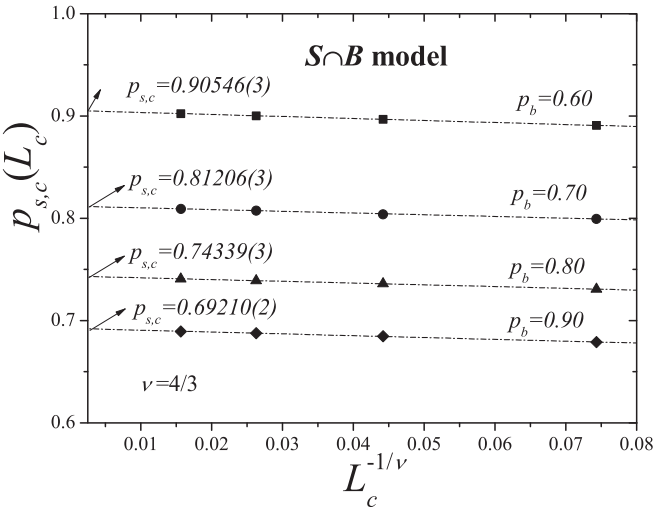

FIG. 3. Extrapolation of $p_{s,c}(L_c)$, towards the thermodynamic limit according to the theoretical prediction given by Eq. (17). The data correspond to the $S \cap B$ model with $p_b = 0.60$ (squares), $p_b = 0.70$ (circles), $p_b = 0.80$ (triangles), and $p_b = 0.90$ (diamonds). The plots were made using the exact critical exponent in two dimensions $\nu = 4/3$.

where A^X is a nonuniversal constant and ν will taken as 4/3 (value corresponding to standard percolation in two dimensions).

As an illustrative example, Fig. 3 shows the plots towards the thermodynamic limit of $p_{s,c}(L_c)$ according to Eq. (17) for the $S \cap B$ model and four values of p_b: $p_b = 0.60$ (squares), $p_b = 0.70$ (circles), $p_b = 0.80$ (triangles), and $p_b = 0.90$ (diamonds). From extrapolations it is possible to determine the percolation thresholds in the thermodynamic limit ($L_c \to \infty$). In this case, the values obtained were $p_{s,c} = 0.905\,46(3)$ ($p_b = 0.60$), $p_{s,c} = 0.812\,06(3)$ ($p_b = 0.70$), $p_{s,c} = 0.743\,39(3)$ ($p_b = 0.80$), and $p_{s,c} = 0.692\,10(2)$ ($p_b = 0.90$).

The procedure in Fig. 3 was repeated for different values of p_b and $S \cap B$ and $S \cup B$ models. The results are collected in Table II and will be discussed in detail in the next section.

IV. SITE-BOND PHASE DIAGRAM: COMPARISON BETWEEN SIMULATION AND THEORETICAL RESULTS

We start this section by analyzing the $S \cap B$ model. In the inset of Fig. 4, the simulation results in Table II (solid circles) are compared with previous data from Ref. [23] (solid triangles). The numerical values obtained in Ref. [23] are compiled in Table III. Circles and triangles determine a critical line separating a percolating (nonshaded area in the figure) from a nonpercolating (shaded area in the figure) region. The agreement between previous and current results is excellent, validating our computational approach and calculation method.

The critical curve extends from the point [$p_s = 1.0$, $p_b = 0.524\,405\,3(3)$] at left, to the point [$p_s = 0.652\,703\,6\ldots$, $p_b = 1.0$] at right. $p_b = 0.524\,405\,3(3)$ [40] [$p_s = 0.652\,703\,6\ldots$ [45]] represents the percolation threshold for the standard bond [site] percolation on a kagome lattice (see Ref. [59]).

TABLE II. Simulation values of (p_s, p_b) for the critical line corresponding to the $S \cap B$ and $S \cup B$ percolation models. Statistical errors are in the last digit and are indicated in parentheses.

Simulation data, this paper			
$S \cap B$		$S \cup B$	
p_b	p_s	p_b	p_s
0.53	0.9854(3)	0.02	0.6463(9)
0.55	0.96604(4)	0.05	0.6483(7)
0.60	0.90546(3)	0.10	0.6389(4)
0.65	0.85519(3)	0.15	0.6326(3)
0.70	0.81206(3)	0.20	0.6160(1)
0.75	0.77556(3)	0.25	0.5927(2)
0.80	0.74339(3)	0.30	0.5608(2)
0.85	0.71626(3)	0.35	0.5176(2)
0.90	0.69210(2)	0.40	0.45812(6)
0.95	0.67097(3)	0.45	0.3717(5)
		0.465	0.3403(3)
		0.485	0.2787(4)
		0.50	0.2266(9)

In the main part of Fig. 4, the results obtained from the analytical approaches developed in Sec. II are compared with the simulation data presented in Sec. III. Open cir-

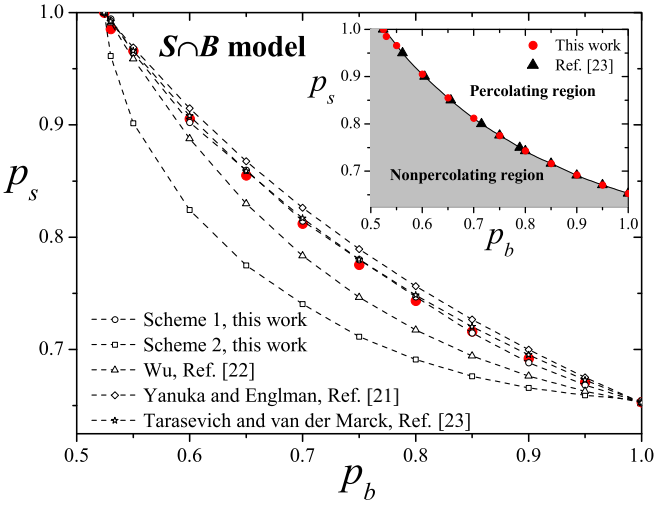

FIG. 4. Analytical and simulation $S \cap B$ phase diagrams for kagome lattices. The symbology is as follows: simulation results in Table II (solid circles); analytical data from scheme 1, first and second columns in Table I (open circles joined by lines); analytical data from scheme 2, fifth and sixth columns in Table I (open squares joined by lines); analytical data from Ref. [22], first and second columns in Table IV (open triangles joined by lines); analytical data from Ref. [21], third and fourth columns in Table IV (open diamonds joined by lines); and analytical data from Ref. [23], fifth and sixth columns in Table IV (open stars joined by lines). In the inset, percolating and nonpercolating regions are indicated. The inset also includes numerical data obtained in the present paper (solid circles) and previous simulations from Ref. [23] (solid triangles).

TABLE III. Simulation values of (p_s, p_b) for the critical line corresponding to the $S \cap B$ percolation model. The data correspond to values taken from Ref. [23]. Statistical errors are in the last digit and are indicated in parentheses.

Simulation data [23] $S \cap B$	
p_b	p_s
0.5615(4)	0.95
0.6046(5)	0.90
0.6556(6)	0.85
0.7152(7)	0.80
0.75	0.7757(8)
0.7894(9)	0.75
0.80	0.7428(5)
0.85	0.7162(5)
0.90	0.6914(5)
0.95	0.6711(4)

cles [squares] joined by lines represent analytical data from scheme 1 [scheme 2] (Table I) and solid circles correspond to simulation results in Table II.

The comparative analysis in Fig. 4 includes the predictions from three previous studies [21–23]. In Ref. [22], the $S \cap B$ critical frontier is determined from the condition

$$1 + 3{p_s}^2(1 - 3p_b + 2{p_b}^3 - {p_b}^4) + {p_s}^3(-3 + 9p_b - 3{p_b}^2 - 12{p_b}^3 + 15{p_b}^4 - 6{p_b}^5 + {p_b}^6) = 0. \quad (18)$$

The first and second columns in Table IV compile the values of (p_b, p_s) obtained by solving Eq. (18) for the same values of p_b used in the numerical simulations. The corresponding results are shown in Fig. 4 as open triangles joined by lines.

The shape of the boundary between percolation and non-percolation was also studied by Yanuka and Englman [21]. The authors proposed the following equation for the $S \cap B$ percolation phase diagram:

$$\frac{\log p_s}{\log p_{s,c}} + \frac{\log p_b}{\log p_{b,c}} = 1. \quad (19)$$

Tarasevich and van der Marck [23] studied the same $S \cap B$ critical curve for different lattices, obtaining the following boundary equation:

$$p_b\left(p_s + \frac{p_{b,c} - p_{s,c}}{1 - p_{b,c}}\right) = p_{b,c}\frac{1 - p_{s,c}}{1 - p_{b,c}}. \quad (20)$$

Equations (19) and (20) were used to calculate the $S \cap B$ phase diagram for kagome lattices. As in previous cases, the values of p_b were chosen according to the p_b concentrations used in the simulations. The results are summarized in Table IV and plotted in Fig. 4 as open diamonds joined by lines [Eq. (19)] and open stars joined by lines [Eq. (20)]. Solving Eqs. (19) and (20) requires the inclusion of $p_{b,c}$ and $p_{s,c}$ as extra parameters. In the case of Table IV and Fig. 4, we take $p_{b,c} = 0.524\,405$ [40] and $p_{s,c} = 0.652\,704$ [45], following the calculations in Ref. [23].

The behavior of the two critical curves introduced in this paper is explained as follows: while the results from scheme 1 (open circles joined by lines) show an excellent agreement with the numerical calculations, scheme 2 (open squares joined by lines) predicts a smaller p_s than the simulation data over the range of p_b. With respect to previous studies, Wu's critical curve (open triangles joined by lines) agrees relatively well with the simulation results for the limit values of p_b ($p_b \to p_{b,c}$ and $p_b \to 1$); however, the disagreement turns out to be significantly large for intermediate values of p_b. Finally, the equations of Yanuka-Englman (open diamonds joined by lines) and Tarasevich–van der Marck (open stars joined by lines) provide good approximations with very small differences between simulation and theoretical results.

The differences between theoretical and numerical data can be easily rationalized with the help of the average relative error E_r, which is defined for each analytical critical

TABLE IV. Values of (p_s, p_b) for the critical line corresponding to the $S \cap B$ and $S \cup B$ percolation models. The data were obtained by following scheme 1 and scheme 2. The values marked with asterisks (∗) and stars (★) were taken from Refs. [40] and [45], respectively, and rounded to five decimal places.

$S \cap B$ model					
Wu [22]		Yanuka and Englman [21]		Tarasevich and van der Marck [23]	
p_b	p_s	p_b	p_s	p_b	p_s
0.52443	1.00	0.52441*	1.00	0.52441*	1.00
0.53	0.99076	0.53	0.99301	0.53	0.99229
0.55	0.95874	0.55	0.96899	0.55	0.96602
0.60	0.88770	0.60	0.91484	0.60	0.90800
0.65	0.82975	0.65	0.86770	0.65	0.85890
0.70	0.78336	0.70	0.82622	0.70	0.81682
0.75	0.74649	0.75	0.78939	0.75	0.78035
0.80	0.71729	0.80	0.75643	0.80	0.74844
0.85	0.69431	0.85	0.72672	0.85	0.72028
0.90	0.67641	0.90	0.69978	0.90	0.69525
0.95	0.66275	0.95	0.67521	0.95	0.67286
1.00	0.65270	1.00	0.65270★	1.00	0.65270★

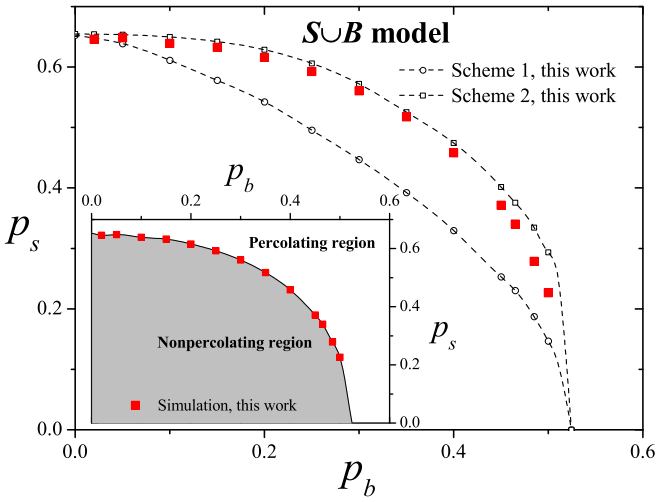

FIG. 5. Analytical and simulation $S \cup B$ phase diagrams for kagome lattices. The symbology is as follows: simulation results in Table II (solid squares); analytical data from scheme 1, third and fourth columns in Table I (open circles joined by lines); and analytical data from scheme 2, seventh and eighth columns in Table I (open squares joined by lines). As in Fig. 4, percolating and nonpercolating regions are indicated in the inset.

curve by

$$E_r = \frac{1}{n}\sum_{i=1}^{i=n}\left|\frac{p^t_{s,i} - p^s_{s,i}}{p^s_{s,i}}\right|_{p_{b,i}}. \tag{21}$$

In the last equation, $p^s_{s,i}$ ($p^t_{s,i}$) denotes the critical fraction of sites calculated from simulation (theoretical approximation). Each pair ($p^s_{s,i}$, $p^t_{s,i}$) is calculated at fixed $p_{b,i}$. n is the number of points in the critical curve.

The average relative error was calculated for the five analytical curves in Fig. 4. The values of $p^s_{s,i}$ were taken from Table II and the values of $p^t_{s,i}$ were taken from Tables I (scheme 1 and scheme 2) and IV (Wu, Yanuka-Englman, and Tarasevich–van der Marck). The obtained results were $E_r = 0.0045$ (scheme 1); $E_r = 0.0628$ (scheme 2); $E_r = 0.0236$ (Wu); $E_r = 0.0121$ (Yanuka-Englman); and $E_r = 0.0046$ (Tarasevich–van der Marck). Appreciable differences can be seen for the different theoretical frameworks, with scheme 1 being the most accurate approximation, predicting the behavior of the $S \cap B$ critical curve in the whole range of (p_b, p_s). In addition, it is important to note that scheme 1 does not require extra parameters, as is the case of the Yanuka-Englman and Tarasevich–van der Marck equations.

On the other hand, the results corresponding to the $S \cup B$ percolation model are shown in Fig. 5: simulation results in Table II (solid squares); analytical data from scheme 1, third and fourth columns in Table I (open circles joined by lines); and analytical data from scheme 2, seventh and eighth columns in Table I (open squares joined by lines). The simulation results are shown again in the inset separating percolating and nonpercolating regions.

As a fundamental difference with previous data in Fig. 4, the critical behavior of the $S \cup B$ model on kagome lattices is reported here. As it is expected, the $S \cup B$ critical curve extends from the point [$p_s = 0.652\,703\,6\ldots$, $p_b = 0.0$] to the

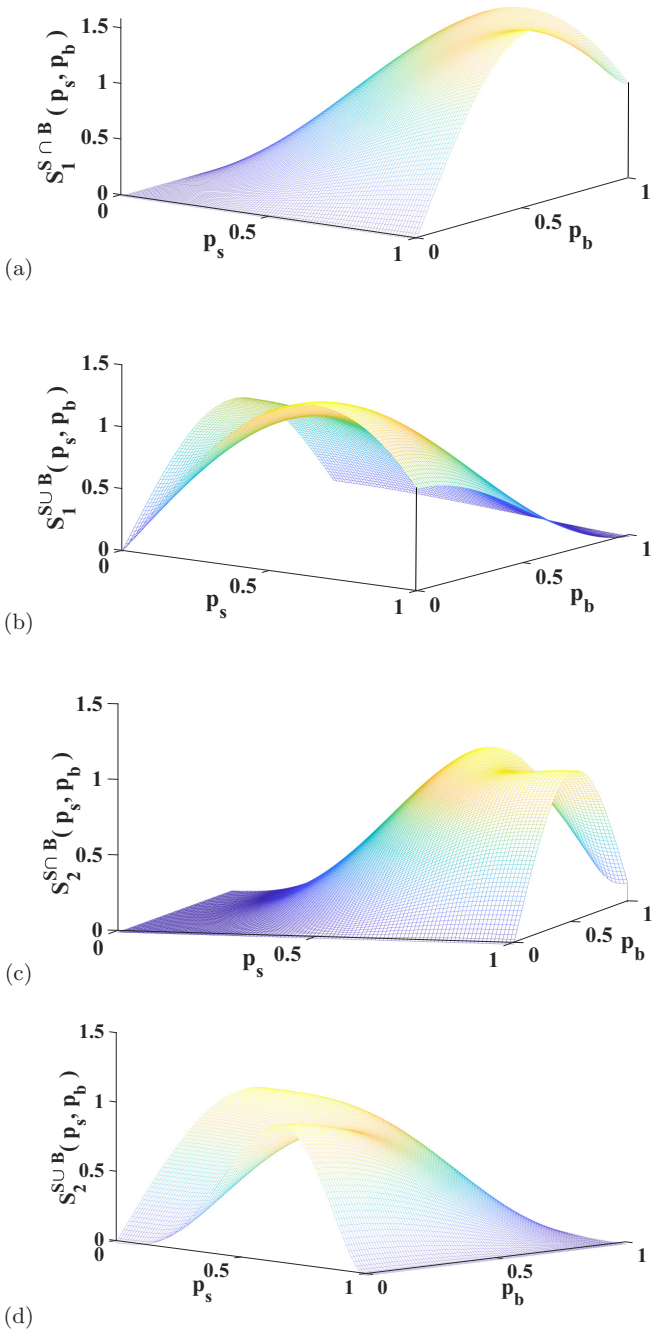

FIG. 6. Gradient norm functions in the (p_s, p_b) plane: (a) $S_1^{S\cap B}$ [Eq. (A3)], (b) $S_1^{S\cup B}$ [Eq. (A4)], (c) $S_2^{S\cap B}$ [Eq. (A3)], and (d) $S_2^{S\cup B}$ [Eq. (A4)].

point [$p_s = 0.0$, $p_b = 0.524\,405\,3(3)$]. Accordingly, the $S \cup B$ critical curve is essentially a continuation of the $S \cap B$ curve (if it is wrapped around the diagram).

With respect to schemes 1 and 2, both approaches show a good qualitative agreement with the simulation data. In the case of scheme 2, an excellent approximation is provided in the range $0 < p_b < 0.4$, and the agreement tends to be worse in the range $0.4 < p_b < p_{b,c}$. On the other hand, scheme 1 predicts smaller values of p_s than the simulation data over the entire range of p_b. The resulting average relative errors are $E_r = 0.1905$ for scheme 1 and $E_r = 0.0650$ for scheme 2,

showing that scheme 2 performs better than scheme 1 for the $S \cup B$ problem.

V. CONCLUSIONS

In this paper, the phase diagram of the site-bond percolation problem for kagome lattices has been addressed. Two distinct schemes, site-and-bond ($S \cap B$) and site-or-bond ($S \cup B$), have been considered. In $S \cap B$, a cluster is considered to be a set of occupied bonds and sites in which the bonds are joined by occupied sites, and the sites are joined by occupied bonds. In $S \cup B$, a bond or site contributes to cluster connectivity independently of the occupation of its end points. Then, by using numerical simulations and finite-size scaling analysis the phase diagrams of the $S \cap B$ and the $S \cup B$ model were determined.

In addition to the simulations, a simple theoretical model was developed. The analytical formalism is based on the well-known Tsallis approximation [52], which allows us to calculate the $S \cap B$ and $S \cup B$ percolation functions from the percolation functions corresponding to pure site and pure bond percolation problems. By using previous theoretical results for pure site and pure bond percolation models in kagome lattices, two analytical schemes were proposed: scheme 1, which combines the Scullard-Ziff solution for pure bond percolation [42] and the Sykes-Essam approach for pure site percolation [45]; and scheme 2, obtained from the mentioned Scullard-Ziff solution [42] and the Rosowsky approximation for pure site percolation [46].

An extensive analysis was carried out for evaluating the present results and comparing them with existing literature [21–23]. In the $S \cap B$ case, the numerical results coincide with previous simulation work [23]. The numerical predictions were also compared with analytical data obtained in the present paper (scheme 1 and scheme 2) and previous theoretical calculations by Wu [22], Yanuka and Englman [21], and Tarasevich and van der Marck [23]. The results of the comparison indicate that scheme 1 allows us to obtain an approximation that is significantly better than the other existing approaches.

On the other hand, the critical curve for the $S \cup B$ model is reported here. A good qualitative agreement is obtained between the simulation and analytical data, with scheme 2 being the most accurate approximation for this case.

In summary, the proposed theoretical framework is simple, is mathematically handleable, and represents a qualitative advance with respect to the existing analytical development of on site-bond percolation in kagome lattices. The present paper complements previous work from our group, where the Tsallis scheme [47] has been successfully applied to two- and three-dimensional Euclidean lattices [50,51]. Future efforts will be directed to extending the analysis to fractal geometries (Sierpinski carpets, DLA clusters, etc.) [60] and random graphs (Erdös-Rényi lattices, random regular graphs, etc.) [61].

ACKNOWLEDGMENTS

This work was supported in part by CONICET (Argentina) under PIP Project No. 112-201701-00673CO and Universidad Nacional de San Luis (Argentina) under Project No. 03-0816. W.L. acknowledges support from Dirección de Investigación Universidad de La Frontera (Chile), under DIUFRO Project No. DI20-0007.

APPENDIX

Once the functions $h_1^{S\cap B}(p_s, p_b)$ [Eq. (10)], $h_1^{S\cup B}(p_s, p_b)$ [Eq. (12)], $h_2^{S\cap B}(p_s, p_b)$ [Eq. (14)], and $h_2^{S\cup B}(p_s, p_b)$ [Eq. (16)] are determined (see Sec. II), the projections of these surfaces on the planes ($p_b = \text{const}$) and ($p_s = \text{const}$) behave in a similar way to the curves of the percolation order parameter obtained with respect to one variable while keeping the second constant. Accordingly, the mentioned projections show a change in the concavity (inflection points), which can be associated to the existence of a transition from a nonpercolating to a percolating state.

A way to study the local curvature of the site-bond percolation functions is by using the concept of gradients. Thus,

$$\begin{aligned}\overrightarrow{\nabla} h_{1\{2\}}^{S\cap B}(p_s, p_b) &= \frac{\partial h_{1\{2\}}^{S\cap B}(p_s, p_b)}{\partial p_s}\widehat{p_s} + \frac{\partial h_{1\{2\}}^{S\cap B}(p_s, p_b)}{\partial p_b}\widehat{p_b} \\ &= \left[g_{\mathrm{SZ}}(p_b)\frac{\partial f_{\mathrm{SE}\{R\}}(p_s)}{\partial p_s}\right]\widehat{p_s} + \left[f_{\mathrm{SE}\{R\}}(p_s)\frac{\partial g_{\mathrm{SZ}}(p_b)}{\partial p_b}\right]\widehat{p_b},\end{aligned} \tag{A1}$$

and

$$\begin{aligned}\overrightarrow{\nabla} h_{1\{2\}}^{S\cup B}(p_s, p_b) &= \frac{\partial h_{1\{2\}}^{S\cup B}(p_s, p_b)}{\partial p_s}\widehat{p_s} + \frac{\partial h_{1\{2\}}^{S\cup B}(p_s, p_b)}{\partial p_b}\widehat{p_b} \\ &= \left[\frac{\partial f_{\mathrm{SE}\{R\}}(p_s)}{\partial p_s} - g_{\mathrm{SZ}}(p_b)\frac{\partial f_{\mathrm{SE}\{R\}}(p_s)}{\partial p_s}\right]\widehat{p_s} + \left[\frac{\partial g_{\mathrm{SZ}}(p_b)}{\partial p_b} - f_{\mathrm{SE}\{R\}}(p_s)\frac{\partial g_{\mathrm{SZ}}(p_b)}{\partial p_b}\right]\widehat{p_b}.\end{aligned} \tag{A2}$$

Now, the norm of the gradients $\|\overrightarrow{\nabla} h_{1\{2\}}^{S\cap B}(p_s, p_b)\|$ and $\|\overrightarrow{\nabla} h_{1\{2\}}^{S\cup B}(p_s, p_b)\|$ can be calculated as

$$\begin{aligned}S_{1\{2\}}^{S\cap B} &= \left\|\overrightarrow{\nabla} h_{1\{2\}}^{S\cap B}(p_s, p_b)\right\| \\ &= \sqrt{\left[g_{\mathrm{SZ}}(p_b)\frac{\partial f_{\mathrm{SE}\{R\}}(p_s)}{\partial p_s}\right]^2 + \left[f_{\mathrm{SE}\{R\}}(p_s)\frac{\partial g_{\mathrm{SZ}}(p_b)}{\partial p_b}\right]^2},\end{aligned} \tag{A3}$$

and

$$S_{1\{2\}}^{S\cup B} = \left\| \overrightarrow{\nabla} h_{1\{2\}}^{S\cup B}(p_s, p_b) \right\| = \sqrt{\left[\frac{\partial f_{\mathrm{SE}\{R\}}(p_s)}{\partial p_s} - g_{\mathrm{SZ}}(p_b) \frac{\partial f_{\mathrm{SE}\{R\}}(p_s)}{\partial p_s} \right]^2 + \left[\frac{\partial g_{\mathrm{SZ}}(p_b)}{\partial p_b} - f_{\mathrm{SE}\{R\}}(p_s) \frac{\partial g_{\mathrm{SZ}}(p_b)}{\partial p_b} \right]^2}. \quad \text{(A4)}$$

$S_1^{S\cap B}$, $S_1^{S\cup B}$, $S_2^{S\cap B}$, and $S_2^{S\cup B}$ are shown in Figs. 6(a)–6(d), respectively. The curves for a fixed value of p_b have a maximum for a given value of p_s, and in the same way the curves for a fixed value of p_s have a maximum for a given value of p_b. The set of such maxima can be calculated by the string method [55,56]. The basic idea of the string method is to find a path of critical points that connect the minimum of the function $V(p_s, p_b) = -S_\alpha^{S\cap B(S\cup B)}(p_s, p_b)$ $(\alpha = 1, 2)$ by evolution of a string of initial points. The string $\{\varphi := (x_i, y_i) \in [0, 1], i = 0, 1, 2, \ldots, s-1\}$ is discretized into $s = 10\,000$ initial points [62] and it evolves until it meets the condition $\overrightarrow{\nabla} V(x_i, y_i)^\perp = 0$, where $\overrightarrow{\nabla} V(x_i, y_i)^\perp$ is the component of $\overrightarrow{\nabla} V(x_i, y_i)$ normal to φ:

$$\overrightarrow{\nabla} V(x_i, y_i)^\perp = \overrightarrow{\nabla} V(x_i, y_i) - [\overrightarrow{\nabla} V(x_i, y_i) \cdot \widehat{t}]\widehat{t}. \quad \text{(A5)}$$

Here $\widehat{t}$ denotes the unit tangent of the curve φ and $\cdot$ denotes the Euclidean inner product. Each point of the curve in evolution moves in the direction of the normal component $\overrightarrow{\nabla} V(x_i, y_i)$ and the tangential component only moves the points along the string keeping the spacing between them. Then, the points are redistributed in every movement. The iteration of the method consists of two steps defined as follows.

(1) Each point of the string initially evolves according to the recurrence equation:

$$x_{i+1} = x_i - \Delta t \frac{\partial V(x_i, y_i)}{\partial p_s}, \quad \text{(A6)}$$

$$y_{i+1} = y_i - \Delta t \frac{\partial V(x_i, y_i)}{\partial p_b}. \quad \text{(A7)}$$

(2) The points along the string are redistributed using a cubic interpolation of the points of the part of the string calculated in each time step Δt.

Finally, when the two end points of the initial string fall in the two minimum points of the function $V(p_s, p_b)$, these points are identified. Then, the critical line is obtained from the path of minimum critical points joining the two minimum end points. The resulting critical curves are shown in Figs. 4 and 5.

[1] J. M. Hammersley and K. W. Morton, J. R. Stat. Soc. B **16**, 23 (1954).
[2] S. R. Broadbent and J. M. Hammersley, Proc. Camb. Phil. Soc. **53**, 629 (1957).
[3] D. Stauffer and A. Aharony, *Introduction to Percolation Theory* (Taylor & Francis, London, 1994).
[4] M. Sahimi, *Applications of Percolation* (Taylor & Francis, London, 1994).
[5] R. Li, Y. S. Yang, J. Pan, G. G. Pereira, J. A. Taylor, B. Clennell, and C. Zou, Phys. Rev. E **90**, 033301 (2014).
[6] B. Vigolo, C. Coulon, M. Maugey, C. Zakri, and P. Poulin, Science **309**, 920 (2005).
[7] C. Grimaldi and I. Balberg, Phys. Rev. Lett. **96**, 066602 (2006).
[8] S. N. Dorogovtsev and J. F. F. Mendes, *Evolution of Networks: From Biological Nets to the Internet and WWW* (Oxford University Press, New York, 2003).
[9] M. E. J. Newman, *Networks: An Introduction* (Oxford University Press, New York, 2010).
[10] R. Cohen and S. Havlin, *Complex Networks, Structure, Robustness and Function* (Cambridge University Press, Cambridge, England, 2010).
[11] S. Lowinger, G. A. Cwilich, and S. V. Buldyrev, Phys. Rev. E **94**, 052306 (2016).
[12] S. G. Anekal, P. Bahukudumbi, and M. A. Bevan, Phys. Rev. E **73**, 020403(R) (2006).
[13] I. A. Gruzberg, A. W. W. Ludwig, and N. Read, Phys. Rev. Lett. **82**, 4524 (1999).
[14] J. C. Miller, Phys. Rev. E **80**, 020901(R) (2009).
[15] G. Grimmett, *Percolation* (Springer-Verlag, Berlin, 1999).
[16] K. Christensen and N. R. Moloney, *Complexity and Criticality* (Imperial College, London, 2005).
[17] B. Bollobás and O. Riordan, *Percolation* (Cambridge University Press, New York, 2006).
[18] H. L. Frisch and J. M. Hammersley, J. Soc. Ind. Appl. Math. **11**, 894 (1963).
[19] P. Agrawal, S. Render, P. J. Reynolds, and H. E. Stanley, J. Phys. A: Math. Gen. **12**, 2073 (1979).
[20] H. Nakanishi and J. Reynolds, Phys. Lett. A **71**, 252 (1979).
[21] M. Yanuka and R. Englman, J. Phys. A: Math. Gen. **23**, L339 (1990).
[22] F. Y. Wu, Phys. Rev. E **81**, 061110 (2010).
[23] Y. Y. Tarasevich and S. C. van der Marck, Int. J. Mod. Phys. C **10**, 1193 (1999).
[24] J. E. Ramírez, C. Pajares, M. I. Martínez, R. Rodríguez Fernández, E. Molina-Gayosso, J. Lozada-Lechuga, and A. Fernández Téllez, Phys. Rev. E **101**, 032301 (2020).
[25] A. Coniglio, H. E. Stanley, and W. Klein, Phys. Rev. Lett. **42**, 518 (1979).
[26] R. M. Ziff, E. Gulari, and Y. Barshad, Phys. Rev. Lett. **56**, 2553 (1986).
[27] C. T. Rettner and H. Stein, Phys. Rev. Lett. **59**, 2768 (1987).
[28] Z. Gao and Z. R. Yang, Physica A **255**, 242 (1998).
[29] J. M. Hammersley, Math. Proc. Camb. Phil. Soc. **88**, 167 (1980).
[30] M. Yanuka, J. Colloid Interface Sci. **134**, 198 (1990).

[31] V. Mayagoitia, F. Rojas, and I. Kornhauser, J. Chem. Soc. Faraday Trans. 1 **81**, 2931 (1985).
[32] R. Englman and Z. Jaeger, Physica A **168**, 655 (1990).
[33] I. Syôzi, Prog. Theor. Phys. **6**, 306 (1951).
[34] G. Xu, B. Lian, and S.-C. Zhang, Phys. Rev. Lett. **115**, 186802 (2015).
[35] W. Zhu, S.-S. Gong, T.-S. Zeng, L. Fu, and D. N. Sheng, Phys. Rev. Lett. **117**, 096402 (2016).
[36] J.-X. Yin *et al.*, Nature (London) **562**, 91 (2018).
[37] T. Kida, L. A. Fenner, A. A. Dee, I. Terasaki, M. Hagiwara, and A. S. Wills, J. Phys. Condens. Matter **23**, 112205 (2011).
[38] K. Kuroda *et al.*, Nat. Mater. **16**, 1090 (2017).
[39] L. Ye *et al.*, Nature (London) **555**, 638 (2018).
[40] R. M. Ziff and P. N. Suding, J. Phys. A: Math. Gen. **30**, 5351 (1997).
[41] C. R. Scullard, Phys. Rev. E **73**, 016107 (2006).
[42] C. R. Scullard and R. M. Ziff, Phys. Rev. E **73**, 045102(R) (2006).
[43] C. R. Scullard and R. M. Ziff, J. Stat. Mech. (2010) P03021.
[44] C. R. Scullard, J. Stat. Mech. (2011) P09022.
[45] M. F. Sykes and J. W. Essam, J. Math. Phys. **5**, 1117 (1964).
[46] A. Rosowsky, Eur. Phys. J. B **15**, 77 (2000).
[47] C. Tsallis and A. C. N. de Magalhães, Phys. Rep. **268**, 305 (1996).
[48] M. Dolz, F. Nieto, and A. J. Ramirez-Pastor, Phys. Rev. E **72**, 066129 (2005).
[49] M. I. González, P. M. Centres, W. Lebrecht, A. J. Ramirez-Pastor, and F. Nieto, Physica A **392**, 6330 (2013).
[50] M. I. González, P. M. Centres, W. Lebrecht, and A. J. Ramirez-Pastor, J. Stat. Mech. (2016) 093210.
[51] L. S. Ramirez, N. De la Cruz Félix, P. M. Centres, and A. J. Ramirez-Pastor, J. Stat. Mech. (2017) 023206.
[52] C. Tsallis, Physica A **344**, 718 (2004).
[53] B. Grünbaum and G. C. Shephard, *Tilings and Patterns* (Freeman, San Francisco, 1987).
[54] For the bond problem, triangular and honeycomb lattices form a matching pair and the critical points are complementary [45].
[55] W. E, W. Ren, and E. Vanden-Eijnden, Phys. Rev. B **66**, 052301 (2002).
[56] W. E, W. Ren, and E. Vanden-Eijnden, J. Chem. Phys. **126**, 164103 (2007).
[57] J. Hoshen and R. Kopelman, Phys. Rev. B **14**, 3438 (1976).
[58] The Hoshen and Kopelman algorithm is used to detect connectivity. For the $S \cap B[S \cup B]$ model, two points are said to be connected if a sequence of occupied sites *and* (*or*) bonds joins them. In both cases, periodic boundary conditions are considered.
[59] See https://en.wikipedia.org/wiki/Percolation_critical_exponents.
[60] S. Havlin, D. Ben-Avraham, and D. Movshovitz, J. Stat. Phys. **36**, 831 (1984).
[61] B. Bollobás, *Random Graphs*, 2nd ed. (Cambridge University Press, Cambridge, England, 2001).
[62] Setting $s = 10\,000$ provides the opportunity to explore many solutions (p_b, p_s) and then to choose those solutions the p_b values of which coincide with the corresponding p_b fractions used in the simulations. This allows for a better comparison between theoretical and numerical results.